FERMILAB-PROPOSAL-0903

903

A TEST EXPERIMENT AT THE FERMILAB BOOSTER TO STUDY THE FEASIBILITY OF FAST ANTIHYDROGEN SPECTROSCOPY

G. Blanford, M. Mandelkern[1], J. Schultz, G. Zioulas
University of California, Irvine

D. Christian, K. Gollwitzer, A. Hahn, F. Nezrick
Fermilab

N. Bigelow, Th. Koffas, P. Londero, A. Melissinos
University of Rochester

C. Munger[2]

March 20, 1998

[1]Spokesperson
[2]Mailing address: SLAC, P. O. Box 4349, Bin 43, Stanford, California, 94309

Abstract

Atomic antihydrogen has recently been observed at Fermilab [1]. It appears feasible to measure the principal structure, fine structure and Lamb shift of antihydrogen atoms in flight [2]. It is possible to test the proposed techniques and measure cross sections for the relevant atomic processes at relativistic velocities by first using a proton beam. We propose to perform such a test at the FNAL Booster using 8 GeV protons, either in the old transfer line from the Booster to the Main Ring (the proposed "silicon damage" test facility) or in the permanent magnet transfer line to the Main Injector.

1. Introduction

CPT invariance is a fundamental assumption of quantum field theory and is widely believed to be an absolute symmetry of nature. The neutral K system provides the most accurate test of CPT invariance in weak interactions; a model dependent estimate of the $K^0\ \overline{K}^0$ mass difference is less than one part in 10^{18}. The equality of proton and antiproton masses is known to one part in 10^9. However there are no tests of CPT invariance in atomic systems since until recently no anti-atoms were observed. CPT predicts that atom and anti-atom energies, moments and lifetimes are equal.

To exploit the high precision of atomic laser spectroscopy the anti-atoms must be trapped. This approach has been adopted by CERN which is in the process of constructing an antiproton decelerator to deliver low momentum antiprotons ($p < 100$ MeV/c)[3]. However formation of **hydrogen** in a trap has not as yet been achieved in spite of substantial efforts. In contrast, background-free fast antihydrogen has been observed at Fermilab by the E-862 collaboration [1]. It is therefore of interest to explore the possibilities for spectroscopy of relativistic antihydrogen atoms.

It has been shown that vacuum oscillations of the $n = 2$ Stark states can be used to measure the fine structure and Lamb shift of antihydrogen [2]. At 8.85 GeV/c, the oscillation length arising from the fine structure energy difference $(2P_{3/2} - 2P_{1/2})$ is 28.5 cm and that related to the Lamb shift $(P_{1/2} - 2S_{1/2})$ is 267 cm. Atoms in excited states are identified by field ionization in a vacuum. Preparation of the long lived (L) Stark state is achieved by exciting the atoms to $n = 2$ states as they pass through a thin foil and then selectively ionizing the short lived (S) and medium lived (M) Stark states. Alternatively we may selectively excite the individual Stark states using a laser. The laser could both allow a direct measurement of the $n = 1 \rightarrow 2$ transition energy and produce a sample of the Stark L state for the vacuum oscillation method.

We propose to test the ideas described above by using the proton beam from the Fermilab Booster to perform spectroscopy on hydrogen atoms in flight in anticipation of an antihydrogen experiment at the Antiproton Source. In particular we wish to:

(a) Measure the excitation and ionization cross sections for relativistic (8.85 GeV/c) hydrogen passing through thin foils. At present only estimates exist for those cross sections.

(b) Demonstrate laser excitation of the $n = 1 \rightarrow 2$ transitions and selective excitation of the $n = 2$L Stark state.

(c) Observe vacuum oscillations of the $n = 2$ Stark states and measure the oscillation frequencies for the fine structure and Lamb shift of hydrogen.

We discuss the experimental set-up and run plan, methods for producing hydrogen atoms and detecting them by ionization, techniques for excitation using thin foils and lasers, and the vacuum oscillation technique. The latter and the feasibility of fast antihydrogen spectroscopy are further discussed in [2].

We anticipate a rate of $\sim 3 \times 10^{12}$ protons/s on target. For operation in the old transfer line from the Booster to the Main Ring a minor redesign of the optics of the charged beam for the silicon radiation damage facility is necessary. A vacuum insertion to accommodate detectors and laser optics will need to be installed and an optical transport line from the laser room to the experiment is required. Installation in the new permanent magnet transfer

line, for example between 810 and 814, would also be possible.

2. Experimental Set-up and Run Plan

The set-up of the experiment in the old transfer line from the Booster to the Main Ring is shown in Fig. 1. Hydrogen is produced in a $\sim$200 μg/cm^2 CH foil and continues in the forward direction. The proton beam is bent away from the neutral beam by vertical dipoles DMP1 and DMP2. After a third vertical bend, the proton beam is dumped underground. Two horizontal dipoles, HB1A and HB1B, are located immediately downstream of DPM2, and are energized to direct beam along the trajectory of the old transfer line from the Booster to the Main Ring for use in the new radiation damage facility. When the radiation damage facility is in use, DMP1 and DMP2 will not be energized. There is approximately 24 m of free space downstream of HB1B suitable for our use. A drift of approximately two meters downstream of HB1B allows the charged radiation damage beamline to separate from the neutral beam. Foil and/or laser excitation is carried out in magnet E1 with magnetic field up to $\sim$1.0 T. After a $\leq$2 m long drift region free of magnetic fields, we have an identical magnet E2 containing an ionizing foil at its downstream end. Both magnets are instrumented to detect the electron from ionization of the hydrogen atom and determine the ionization point. Finally we have a spectrometer to identify the protons from the ionization, consisting of dipoles D3 and D4 and wire chambers.

The Booster proton beam has the same momentum as the Source antiproton beam with comparable momentum width and transverse emittance. The relatively large cross section for hydrogen formation by electron capture (inverse photoelectric effect) at 8.85 GeV/c is $344Z$ pb [5]; for carbon $\sigma \sim 2 \times 10^{-33}$cm^2. By extrapolation of low energy data the stripping cross section for hydrogen is $\sim 2 \times 10^{-19}$cm^2. As shown below, using a thick target ($t \gg 100\mu$g/cm^2) yields 10^{-14} hydrogens per incident proton. For an incident flux of 3×10^{12} per second we obtain $\sim$2,000 hydrogen atoms/day.

We prepare the Stark L state by passing the beam through a thin foil ($\sim 70\mu$g/cm^2) placed in magnet E1. As shown below, at least 8% of the hydrogen atoms are excited with equal probability to all $n = 2$ states, giving $\geq$2% of the sample in the L state. Most S and M atoms ionize in magnet E1 and are counted. For an effective regeneration distance of 30 cm, $\sim$90% of the L atoms oscillate into S and ionize in magnet E2, giving $\sim$30 events/day for an adequate measurement of the excitation cross section and a demonstration of vacuum oscillation. $n = 1$ atoms ionize in the foil in magnet E2 and are counted.

We may then observe the evolution in free space of the L state by counting the S and M atoms that ionize in magnet E2 as a function of regeneration distance. It may be possible to vary the effective regeneration distance by introducing magnetic fields between E1 and E2 instead of moving either magnet. The free space evolution depends only on the fine structure and Lamb shift.

We will study optical excitation of hydrogen using a laser-driven high-Q Fabry-Perot cavity, placed in magnet E1 which is set to a field sufficient to separate the S, M and L states by more than the beam momentum width. Without a field, the hydrogen fine structure cannot be resolved. S, M and L are selectively excited and are detected using their characteristic ionization patterns in magnets E1 and E2. The excitation frequency is tuned by varying the angle between the laser and the neutral beam. For example, in order to find

the correct angle (frequency) when tuning for the L state, the field in magnet E2 is set high enough so that all three Stark states ionize. We will measure the transition energies from the ground state to S, M and L, determining the principal and fine structure of $n = 2$ hydrogen. We estimate 14% (26%) selective excitation to the $n = 2$ S and L (M) Stark states, for ~250 (500) detected events/day. Measurement of the M transition, where only a quadratic Stark shift is present, will give a measurement of the Rydberg, R_y , at a level $\leq 10^{-4}$. We will obtain ~250 events/day for the study of vacuum oscillations of the L state.

An alternative spectroscopic method involves increasing the field in magnet E1 so that the $n = 2$ Stark states are broadened to match the laser Doppler broadening by being strongly coupled to the continuum. Excitation is immediately followed by ionization; this is equivalent to a 2-photon transition and is discussed below. All three Stark states can be studied this way.

The proton spectrometer (shown schematically in Fig. 2) will include the existing wire chambers and counters from E-862. Two 5-foot long magnets previously used in the old transfer line will give a 5° bend and a resolution $\sigma_p/p < 10^{-3}$ for a 40 ft. length.

The 4.8 MeV ionization electron has a 2.0 cm radius in the 0.8 T field in which it is produced. A suitable detector is an active vertical plane 2 cm from the neutral beam center line and parallel to the beam line. An ionization occurring within 2 cm from the beam center line is detected as the electron's helical orbit passes through the detector. The mean longitudinal (z) coordinate of the first two intersections of the electron orbit gives the ionization point. For all of the detector technologies that we have considered, the z error is determined by multiple scattering and is less than 1 mm. In order to facilitate pattern recognition, it may prove desirable to incline the magnetic field with respect to the beam direction so that the direction of the electron spiral will always be the same.

One possible electron detector is a vertical silicon strip detector 30 cm long (beam direction) with strips 2 cm high. Readout at 1 mm z intervals giving 300 channels is adequate. Another possibilty is a PWC of similar dimension and readout pitch. A third possibility is a silicon drift detector [4], such as is currently being built for STAR at RHIC. The pattern recognition power of the silicon drift detector makes it an especially attractive alternative.

3. Cross Sections and Rates for Hydrogen Production and Foil Excitation

We consider hydrogen formation and excitation to $n = 2$ in thin foils. The formation cross section is predicted to be $344Z$ pb [5]. Excitation and ionization cross sections at 8 GeV are not known and an accurate theoretical treatment is not available. However a theoretical treatment of H^- stripping in carbon foils [6] applied to data obtained at 800 MeV [7] offers some guidance. Unfortunately that experiment does not resolve $n = 1$ and $n = 2$ hydrogen which limits its usefullness. Yields are mainly sensitive to ratios of cross sections. Cross sections are taken to scale as $\frac{1}{\beta^2}$, an assumption that is supported by recent theoretical work [8].

A proton beam at rate N_p incident on a foil of thickness t forms $n = 1$ hydrogen with cross section σ_f; $n = 1$ hydrogen ionizes with cross section σ_1. The $n = 1$ rate is:

$$N_1 = N_p \frac{\sigma_f}{\sigma_1}(1 - e^{-n\sigma_1 t}).$$

The thick target rate is:

$N_{1t} = N_p \frac{\sigma_f}{\sigma_1}$.

For $N_p = 3 \times 10^{12}$ s^{-1}, $\sigma_f = 344Z$ pb=2 nb, $\sigma_1 = 2 \cdot 10^{-19}$ cm^2, giving N_{1t}=0.03 s^{-1}.

Hydrogen in $n = 1$ at rate N_1 incident on a foil of thickness d is excited to $n = 2$ with cross section σ_e; hydrogen in $n = 2$ ionizes with cross section σ_2. The $n = 2$ rate is:

$$N_2 = \frac{N_1 \sigma_e}{\sigma_2 - \sigma_1 - \sigma_e} \left\{ e^{-n\{\sigma_1 + \sigma_e\}d} - e^{-n\sigma_2 d} \right\}$$

We obtain a maximum rate, N_{2m} for

$$t_m = \frac{ln(\frac{\sigma_2}{\sigma_1 + \sigma_e})}{n(\sigma_2 - \sigma_1 - \sigma_e)}$$

Following [6], we take $\frac{\sigma_e}{\sigma_1} \simeq 1/3$ and $\frac{\sigma_1}{\sigma_2} \simeq 1$, and find that $t_m \simeq 87 \mu$g/cm^2 and $\frac{N_{2m}}{N_1} \simeq 0.12$. If we double σ_2, $t_m \simeq 70 \mu$g/cm^2 and $\frac{N_{2m}}{N_1} \simeq 0.08$.

An excitation yield of 0.1, as reported at 350 MeV/c [11] is plausible for our conditions. For the antihydrogen experiment it is important to know the excitation and ionization cross sections in order to choose suitable production and excitation foils. By taking data with several foils, we will measure these in the Booster experiment.

4. Optical Excitation

It is possible to carry out optical excitation of relativistic hydrogen in flight. Important considerations are: (1) The atoms spend a very short time in the optical field (2) There is a large spread in the Doppler shift due to the momentum and angular width of the beam. We take $\sigma_p/p = 3.5 \times 10^{-4}$ and $\sigma_\theta = 1.2 \times 10^{-4}$ r [12]. (3) The experimental conditions and high velocity of the atoms make it impractical to efficiently detect the radiative decay, so that ionization must be used as the signal for excitation.

We propose to measure the excitation energies from the ground state to the $n = 2$ Stark states in an electric field, and will also use the laser field to selectively excite the L Stark state for the oscillation experiment. Due to the relativistic motion of the hydrogen atoms, the laser frequency $\overline{\omega}$ seen in the H rest frame is related to the laser frequency ω_0 in the laboratory by

$$\overline{\omega} = \gamma \omega_0 (1 + \beta \cos\theta) \tag{1}$$

Here β, γ refer to the H atom, and θ is the angle between the laser and the H atom direction. We will use a Nd:YAG laser $\lambda = 1064$ nm, $\omega_0 = 1.77 \times 10^{15}$ s^{-1} to excite the $n = 1 \rightarrow 2$ transitions of hydrogen, which occur (for zero E-field) at $\lambda = 121$ nm. Since the H momentum is fixed at $p_H = 8.85$ GeV/c ($\gamma = 9.49$, $\beta\gamma = 9.43$), the crossing angle for 121 nm is given by

$$\cos\theta = -0.074 \qquad \theta = 94.24^\circ \tag{2}$$

Scanning in frequency is achieved by rotating the laser beam with respect to the H direction.

In order to achieve the desired photon density the laser beam is incident on a Fabry-Perot (F-P) optical cavity with $Q = 3.0 \times 10^{10}$. Thus the radiation is highly monochromatic; since

$\nu = 2.82 \times 10^{14}$ Hz, $\Delta_\nu = \nu/Q = 10$ kHz where Δ signifies fwhm. On the other hand the H atoms have $\sigma_p/p \simeq 3.5 \times 10^{-4}$ whereas the natural width of the transition is

$$\Gamma_R = \frac{1}{\tau_{2P\to 1S}} = 6.3 \times 10^8 \text{ s}^{-1} \qquad \left(\frac{\Delta_E}{E}\right)_R = \frac{\Gamma_R}{\overline{\omega}} = 4 \times 10^{-8} \tag{3}$$

Consequently, on average, the frequency seen in the H rest frame is detuned from the resonance frequency by 2×10^4 line widths, completely preventing absorption of the laser photons.

To overcome this problem the F-P cavity consists of convex and concave concentric mirrors as shown in Fig. 3. The radius of curvature is 10 m which introduces an angular divergence $\Delta_\theta = 10^{-3}$ r for a 0.5 cm radius beam. It is clear from Eq. (1) that the angular divergence will effectively broaden the laser line in the H-atom's rest frame to match the momentum spread.

We estimate the transition probabilities in an electric field below the ionization threshold. The Stark states are approximated as linear sums of $n = 2$ vacuum states. We take the laser light approximately normal to the atomic beam and applied magnetic field. For S or L excitation the peak cross section for light polarized in the beam direction is

$$\sigma_{1S\to L,S} = 6\pi\lambda^2 \frac{1}{2} = 3.50 \times 10^{-11} \text{cm}^2 \tag{7}$$

where $\lambda = 121$ nm and $1/2$ results from the $1/\sqrt{2}$ projection of these states onto $2P(m = 0)$. For the degenerate M states, which are pure $2P(m = \pm 1)$, the peak cross section for exciting one linear combination by light polarized normal to the beam direction is

$$\sigma_{1S\to M} = 6\pi\lambda^2 = 6.99 \times 10^{-11} \text{cm}^2 \tag{8}$$

The hydrogen atoms traverse the F-P cavity where the laser beam diameter is $D = 1$ cm and the plate separation is $L = 5$ cm. For a reflectivity $R = 0.99999$ (note that F-P mirrors with even higher reflectivity, $R = 0.999995$ are commercially available [9]) we find a finesse

$$F = \pi/(1 - R) = 3 \times 10^5 \tag{9}$$

and

$$Q = 2F(L/\lambda) = 3 \times 10^{10} \tag{10}$$

If the incident laser power is $P = 10$ W, then the stored photon density in the cavity is

$$\rho_\omega = \frac{U}{V}\frac{1}{(\hbar\omega_0)} = \frac{PQ}{V\omega_0}\frac{1}{\hbar\omega_0} = 1.8 \times 10^{14} \text{ cm}^{-3} \tag{11}$$

The laser light in the atomic rest frame is Doppler broadened to $\frac{\Delta_{\overline{\omega}}}{\overline{\omega}} = 8 \times 10^{-4}$ compared to the natural width $\frac{\Gamma_R}{\overline{\omega}} = 4 \times 10^{-8}$ and only half of the photons propagate in the correct direction. In calculating the transition probability we find

$$W = \frac{1}{2}\rho_\omega \frac{\Gamma_R}{\Delta_{\overline{\omega}}} \ell\sigma = 0.15$$

for the L or S state and $W = 0.30$ for the M state, and excitation of 14% (26%) of the L,S (M) H atoms in a 1 cm path length.

An alternate approach to spectroscopy is to couple the n=2 states to the continuum through a strong electric field and use a parallel plate F-P cavity. The E-field seen in the rest frame of the H as it traverses a laboratory magnetic field is

$$E^* = c\gamma\beta B \sim 2 \times 10^9 \text{ V/m} \tag{4}$$

for $B = 0.7$ T. In this field the three n=2 Stark states are separated by $\Delta E \sim 0.3$ eV and have significant probabilities for ionization. We designate the width for ionization by Γ_I; as before Γ_R is the radiative width for the 2P$\rightarrow$1S transition. The electric field is adjusted so that the Stark state of interest has a relative width that matches Δ_p/p. We require

$$\Gamma_I/\Gamma_R = 2.0 \times 10^4$$

or

$$\Gamma_T = \Gamma_I + \Gamma_R \simeq \Gamma_I = 1.26 \times 10^{13} \text{ s}^{-1} \tag{5}$$

and

$$\frac{\Delta_{\overline{\omega}}}{\overline{\omega}} = \frac{\Gamma_T}{\overline{\omega}} = 8 \times 10^{-4} \tag{6}$$

This assures that the frequency width of the incident radiation matches the width of the transition spectrum for $\Delta_p/p = 8 \times 10^{-4}$.

In the presence of the field, excitation to the n=2 state is immediately followed by ionization, thus providing a detection signal. We can think of the process as a 2-photon excitation, where the 2$^{\text{nd}}$ photon is virtual and is provided by the B-field (or E^*-field). This is sketched in Fig. 4.

In this case the transition width is broadened to match the Doppler width of the beam and the cross sections therefore reduced by a factor $\frac{\Gamma_R}{\Gamma_I} = 0.5 \times 10^{-4}$. The entire photon flux going in the correct direction can now excite the transition so the excitation rates are the same as estimated above.

Doppler broadening due to the angular divergence of the beam, estimated as $\sigma_\theta = 1.2 \times 10^{-4}$ r is significantly smaller than that due to the momentum spread.

It may be convenient to search for the excitation lines using the Stark broadened states. The line width in terms of the laser angle is $\Delta_\theta = 8 \times 10^{-4}$ r. The search for the resonant condition is achieved by rotating the F-P with respect to the hydrogen beam. The three Stark levels are split by 1.8° in a field $B = 0.7$ T. We propose to scan at a rate of ~ 1 mr/hour. Since the survey should place us within ± 10 mr of the correct angle, the scan can be completed rapidly; Once the resonance has been located by ionization in the field of E1 we would reduce the B-field in E1, adjust the angle and verify that excited states are produced by observing ionizations in E2.

The realization of a stable F-P cavity with 10 W input and 10 kHz bandwidth requires that the laser frequency be stabilized accordingly. This is achieved by "locking" the laser onto the cavity by active feedback. A scheme using the Pound-Drever technique [10] is shown in Fig. 5. A $Q = 5 \times 10^{11}$ has been achieved with this arrangement for a long cavity $L = 1.75$ m but for an incident power of only 10 mW [9]. Our proposed $Q = 3.0 \times 10^{10}$ and $L = 5$ cm greatly simplify stability and alignment problems so that we should be able to reach the increased power level. The stability of the cavity and of laser pointing are

extremely important. As the F-P cavity is rotated the laser pointing must track the cavity axis. Temperature stability and absence of dust on the cavity mirrors must be guaranteed.

Since the laser cannot be placed adjacent to the interaction region a suitable transport system will have to be installed. The transport elements must be remotely controlled and viewed by IR cameras for adjustment. Feedback with quadrant diodes will be implemented. The F-P itself will be monitored through the reflected and transmitted light. We currently own a Quantronix lamp pumped Nd:YAG 10 W laser which will be used for preliminary tests of the F-P cavity, optical transport line and feedback. To carry out the experiment however, it is necessary to use a diode pumped Nd:YAG 10 W laser which has much lower noise than the lamp pumped laser.

5. Spectroscopy using Vacuum Oscillations

An atom in a 8.85 GeV/c beam that passes through a transverse laboratory magnetic field $B \sim 0.7\,\mathrm{T}$ sees in its rest frame a large electric field $E = \beta\gamma cB \sim 2 \cdot 10^9\,\mathrm{V/m}$. In such a field the $n = 2$ level of hydrogen splits into three levels, each with a different rate of field ionization. The lifetimes of the levels are roughly in the ratios of 25:5:1, and we label the levels as long, medium, and short (lived), respectively. The effects of different laboratory magnetic fields on the rest wavelength and linewidth of the three n=1 $\rightarrow$ 2 transitions, calculated by summing series expansions[13] in powers of the rest-frame electric field, are displayed in Figs. 6 and 7. By using a laboratory magnetic field to prepare a beam of the $n = 2$ long state, we can observe vacuum oscillations and obtain a measurement of the Lamb and fine-structure splittings of the zero-field $n = 2$ states. The technique is described in detail elsewhere[2]; here we present a brief summary. We describe the experiment for hydrogen.

From a beam of $n = 1$ hydrogen we can make a beam whose only excited atoms are in the long level. We may do this either by passing the beam through a target to excite the various $n = 2$ levels, and ionizing the short and medium levels in a 0.7 T magnetic field; or by pumping only the long level with a laser. In this field, the long and medium levels are separated by ~ 100 times the rms Doppler spread for a beam with $\sigma_p = 3.5 \times 10^{-4}$. If this beam suddenly enters a 'drift' region of zero magnetic field, a long state projects onto the zero-field hydrogen eigenstates as

$$\Psi(t{=}0) = \sqrt{\tfrac{1}{2}}|s_{1/2}\rangle + \sqrt{\tfrac{1}{6}}|p_{1/2}\rangle - \sqrt{\tfrac{1}{3}}|p_{3/2}\rangle \ . \tag{1}$$

The state then evolves forward in time as

$$\begin{aligned} \Psi(t) = \quad & \sqrt{\tfrac{1}{2}}e^{-iE(s_{1/2})t/\hbar}|s_{1/2}\rangle \\ + \quad & \sqrt{\tfrac{1}{6}}e^{-iE(p_{1/2})t/\hbar-(\Gamma/2)t/\hbar}|p_{1/2}\rangle \\ - \quad & \sqrt{\tfrac{1}{3}}e^{-iE(p_{3/2})t/\hbar-(\Gamma/2)t/\hbar}|p_{3/2}\rangle \ . \end{aligned} \tag{2}$$

Here Γ is the width (fwhm) of the $2p$ state due to its radiative decay.

The state that is pure long at $t = 0$ evolves into a superposition of long, medium, and short. The probabilities that an initial long state is found in the long, medium, or short level

depend on the time spent in zero field and on the Lamb and fine-structure splittings of the zero-field $n = 2$ states as

$$P\begin{pmatrix}\text{long}\\ \text{short}\end{pmatrix} = \left[\tfrac{1}{2} \pm \quad e^{-x/2}\left(\tfrac{1}{3}\cos fx + \tfrac{1}{6}\cos lx\right)\right]^2 + \left[\quad e^{-x/2}\left(\tfrac{1}{3}\sin fx - \tfrac{1}{6}\sin lx\right)\right]^2 \tag{3}$$

and

$$P(\text{medium}) = \tfrac{2}{9}e^{-x}(1 - \cos(f + l)x)\ , \tag{4}$$

where $x = \Gamma t/\hbar$ and

$$\begin{aligned} l &= (E_{s_{1/2}} - E_{p_{1/2}})/\Gamma > 0\ ; \quad \text{and} \\ f &= (E_{p_{3/2}} - E_{s_{1/2}})/\Gamma > 0\ . \end{aligned} \tag{5}$$

These oscillating functions are plotted in Fig 8. The fast oscillation, of period 28.5 cm, in the probability of a long state is due to the $2s_{1/2}$–$2p_{3/2}$ splitting, and the slow modulation, of period 267 cm, is due to the Lamb shift splitting.

Since the long state can oscillate into a virtually pure short state, and since the ionization rates of these states differ by a factor of roughly 25, the oscillation is easy to detect. The different probability distributions for the point of ionization of a long, medium, and short states in a model magnet placed downstream of the drift region are shown in Fig. 9. Measurement of the distribution of ionization as a function of the time spent in zero field allows extraction of the Lamb and fine-structure splittings of the $n = 2$ levels. Similar oscillations in zero field have been used by Sokolov and Yakovlev [14] to measure the hydrogen Lamb shift to 1.8 ppm using a 20 keV beam, and by Parkhomchuk[11] to measure the Lamb shift to $\sim 1\%$ using a 66 MeV beam ($v/c = 0.35$).

In practice the magnetic field in the drift region is not strictly zero, nor do real magnetic fields have edges that are step-functions. The effect of these departures from ideal are analyzed in Ref. [2]. Briefly, in the drift region the transverse magnetic field must be ≤ 3 mG to avoid Stark mixing; the longitudinal magnetic field must be ≤ 10 G; and it is necessary that the fall of the magnetic field in the range 3 G to 3 mG occur over a distance short compared to the spatial period of the fine-structure oscillation, or 28.5 cm. Magnetic fields 3 G and below can be shaped suitably using μ-metal.

This method is capable of measuring both the Lamb shift to a statistical precision of 5% and the fine-structure splitting to 1% given as few as 100 atoms prepared in the long state. For the details of the analysis that supports this, at first sight surprising, conclusion, see Ref. [2].

References

[1] G. Blanford, D. C. Christian, K. Gollwitzer, M. Mandelkern, C. T. Munger, J. Schultz, and G. Zioulas, "Observation of Atomic Antihydrogen," FNAL-Pub-97/398/E, Phys. Rev. Lett. (in press). CERN experiment PS-210 has reported an observation of antihydrogen, G. Baur et al., Phys. Lett. **B368**, 251-258 (1996).

[2] G. Blanford, K. Gollwitzer, M. Mandelkern, J. Schultz, G. Takei, G. Zioulas, D. C. Christian and C. T. Munger, " Measuring the Antihydrogen Lamb Shift with a Relativistic Antihydrogen Beam," FNAL-Pub-97/426-E, Phys. Rev. D (in press), available at http://publish.aps.org/eprint/gateway/eplist/aps1997dec17_008.

[3] A description of the CERN Antiproton Decelerator (AD) Project is available at http://www.cern.ch/PSdoc/acc/ad/index.html

[4] R. Bellwied et al., Nuc. Inst. Meth. **A377**, 387-392 (1996).

[5] Computed using the Sauter formula, 9.51 on p.266 in Eichler, J. and Meyerhof, W., Relativistic Atomic Collisions, Academic Press, 1995.

[6] M. S. Gulley et al., Phys. Rev. **A53**, 3201-3210 (1996).

[7] B. Gervais et al., Phys. Rev. **A53**, 3189-3200 (1996).

[8] P. Kurpick, C. Reinhold, J. Burgdorfer, B. Gervais, "Excited State Subshell Populations of Hydrogen Atoms after Transmission of Relativistic H^- ions through Thin Foils. Submitted.

[9] A. M. DeRiva et al., Rev. Sci. Instr. **67**, 2680 (1996).

[10] R. W. P. Drever et al., Appl. Phys. **B31**, 97 (1983).

[11] V. V. Parkhomchuk, Hyperfine Interactions **44**, 315 (1988).

[12] FNAL Run II Handbook, available at http://www-bd.fnal.gov/lug/runII_handbook/RunII_index.html.

[13] H. J. Silverstone, E. Harrell, and C. Grot, Phys. Rev. A **24**, 1925 (1981); H. J. Silverstone, Phys. Rev. A **18**, 1853 (1978).

[14] Yu. L. Sokolov and V. P. Yakovlev, Zhurnal Eksperimental noi i Teoreticheskoi Fiziki **83**, 15 (1992)(English translation: Sov. Phys. JETP**56**, 7(1992)); Yu. L. Sokolov, "Interference of the Hydrogen Atom States (n=2)," in *The Hydrogen Atom*, G. F. Bassani, M. Inguscio, and T. W. Hänch, eds., Springer-Verlag Berlin, Heidelberg, 1989, p. 16.

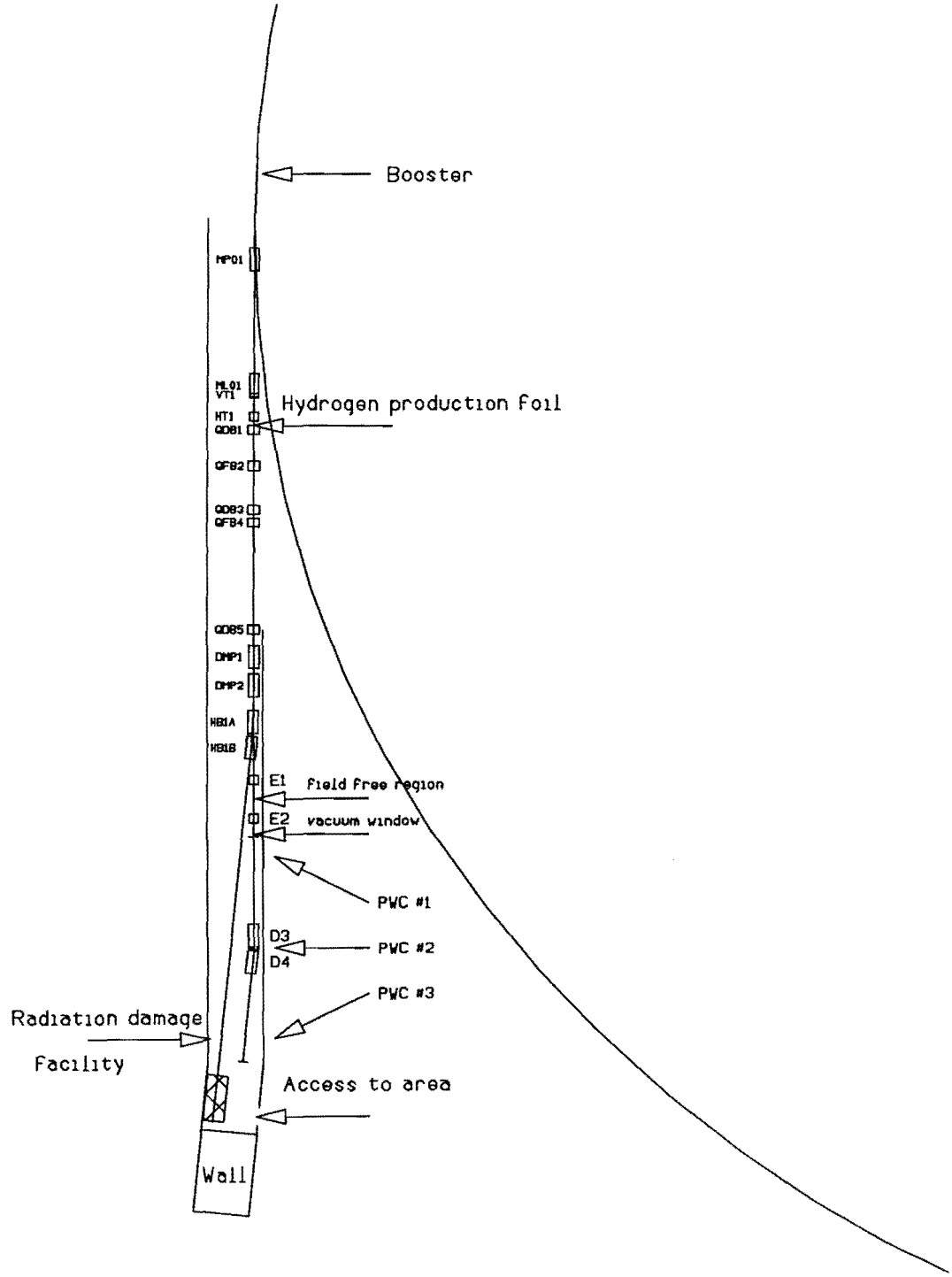

Figure 1: The experimental area in the Booster transfer line.

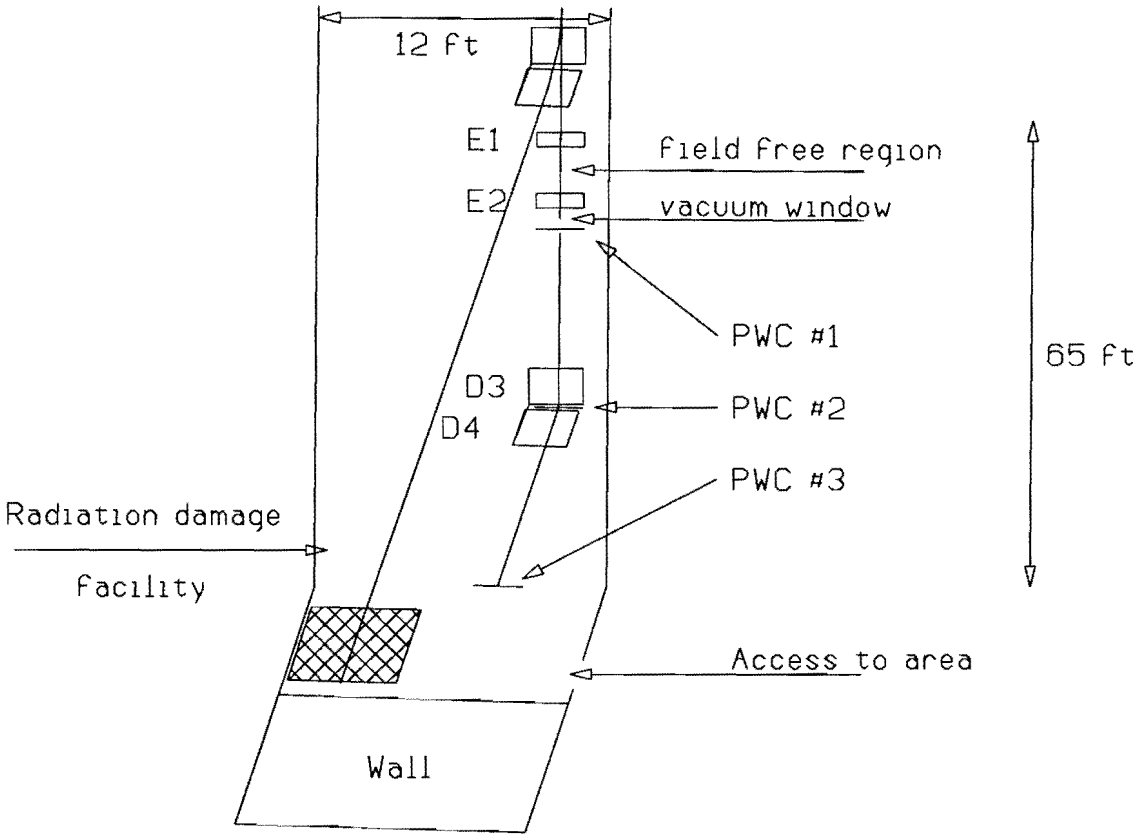

Figure 2: Layout of the hydrogen spectroscopy experiment.

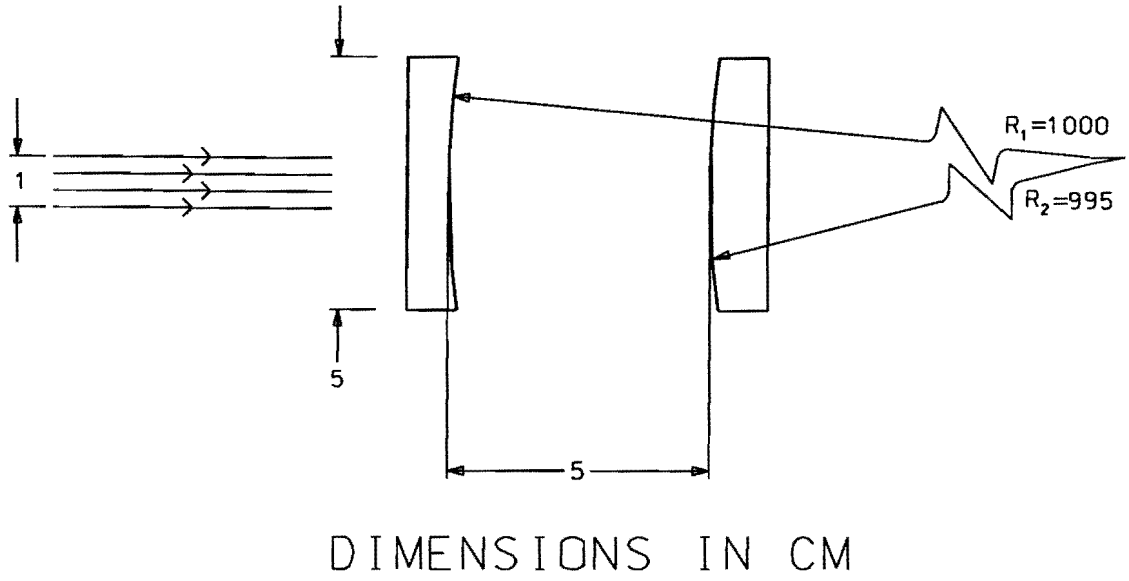

Figure 3: A concentric spherical Fabry-Perot cavity.

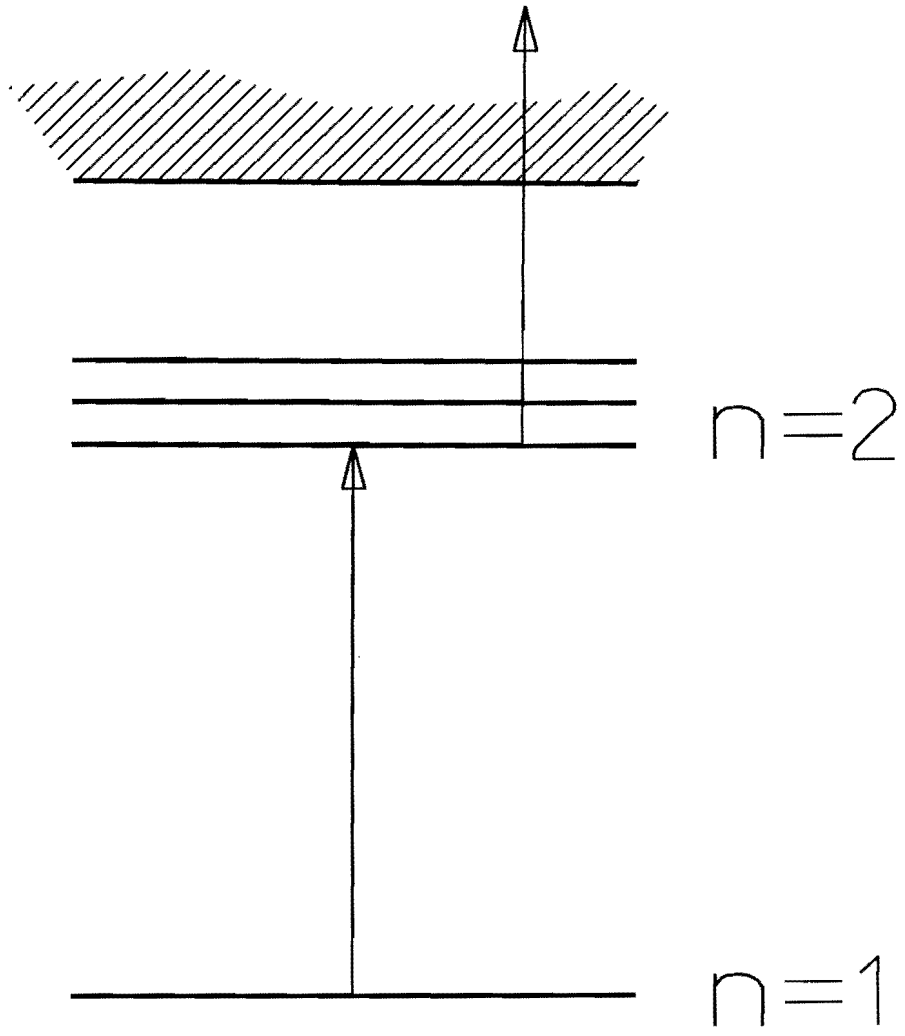

Figure 4: 2-photon ionization using the $n = 2$ Stark states as the intermediate level.

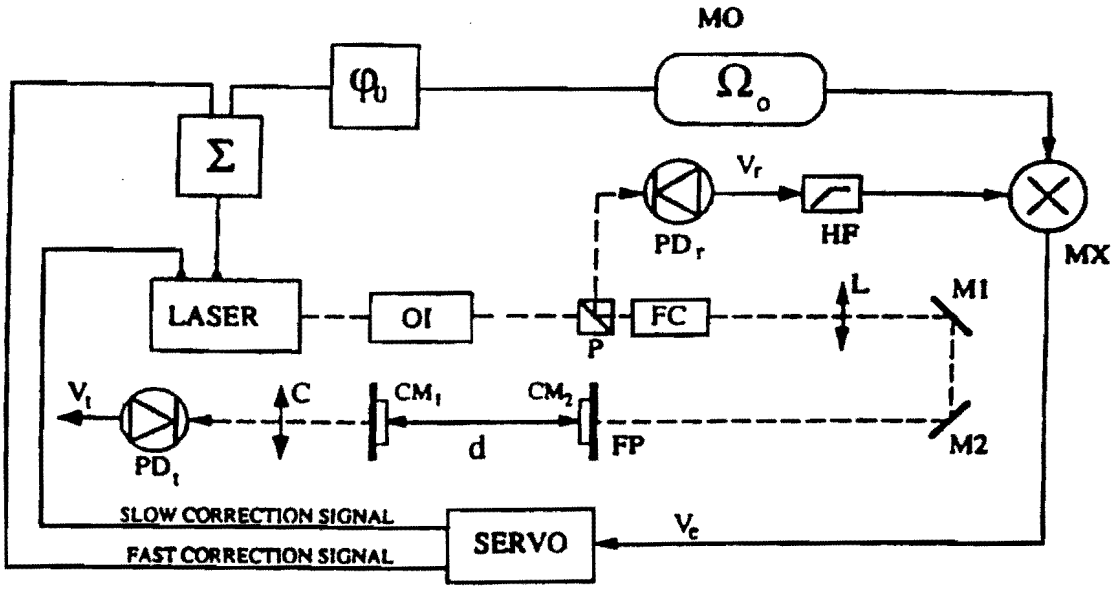

Figure 5: Schematic of a Pound-Drever laser stabilization scheme.

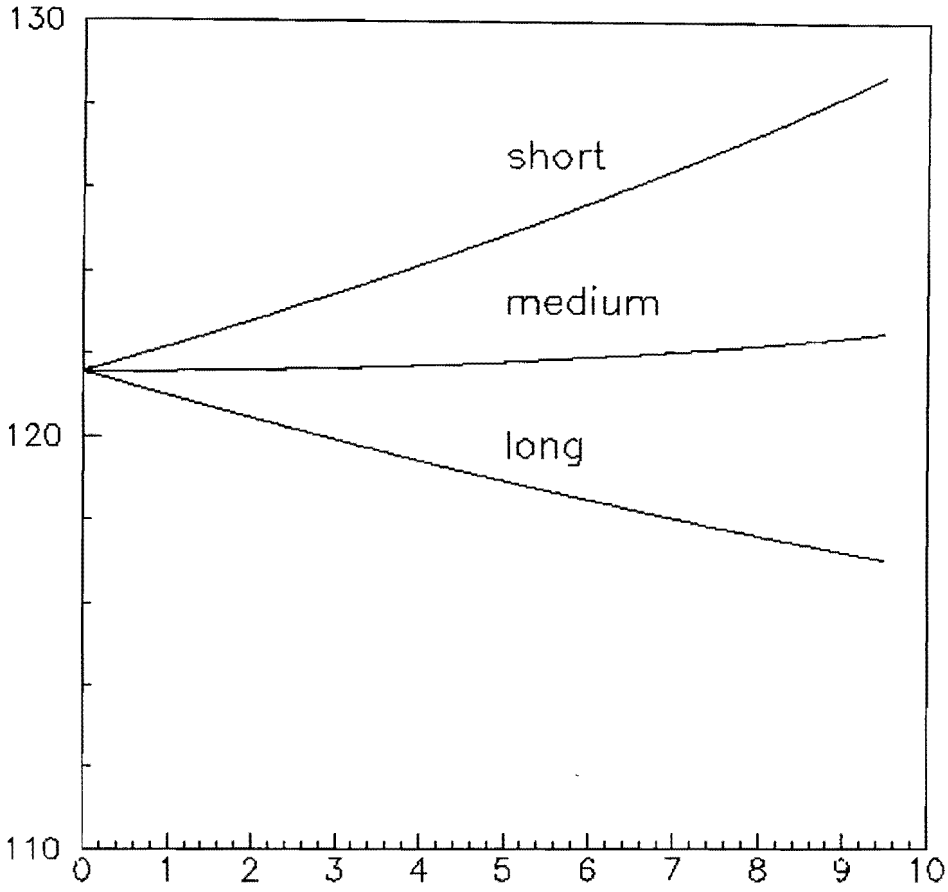

Figure 6: Rest-frame wavelength (nm) of n=1 $\rightarrow$ 2 transitions for an 8.85 GeV/c hydrogen beam, vs. the laboratory transverse magnetic field in kG. The transitions are labeled according to the relative length of their lifetimes in large fields due to field ionization.

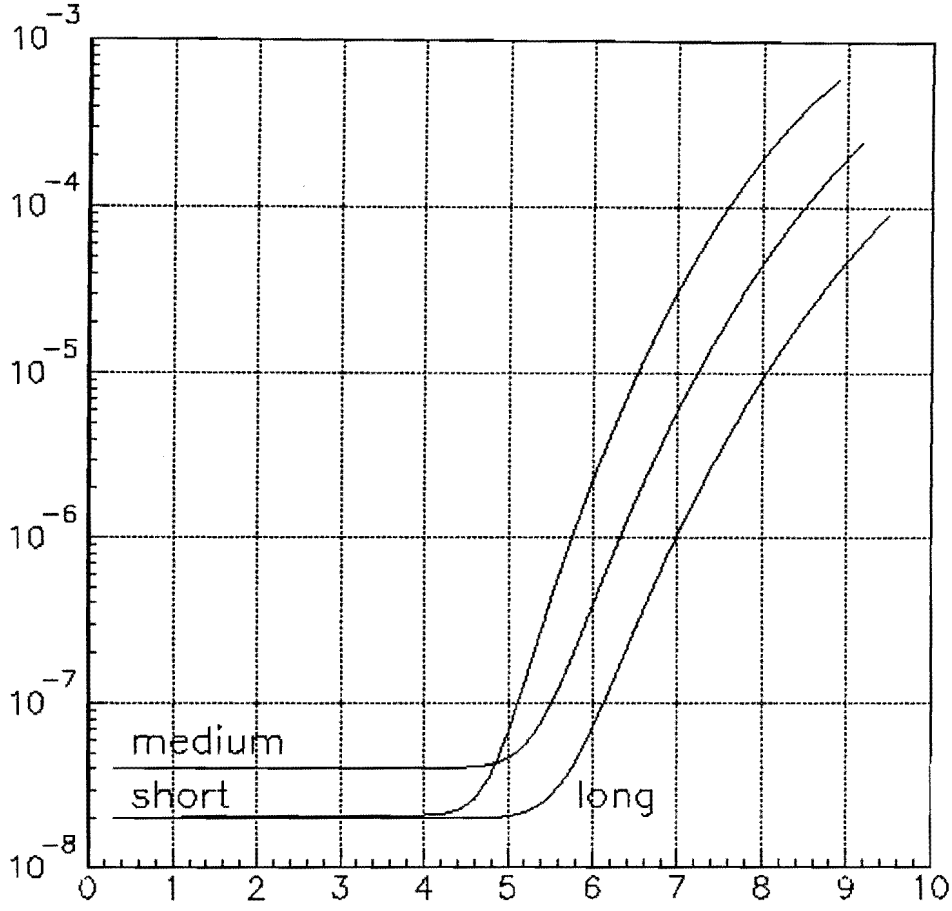

Figure 7: The ratio $\hbar\Gamma/\Delta E$, as seen the the hydrogen rest frame, for the three n=2 $\rightarrow$ 1 transitions as a function of the laboratory transverse magnetic field in kG. Here ΔE is the transition energy and Γ is the decay rate of the n=2 level. At fields below 5 kG the decay rate is dominated by radiative decay, and at fields above 5 kG it is dominated by field ionization.

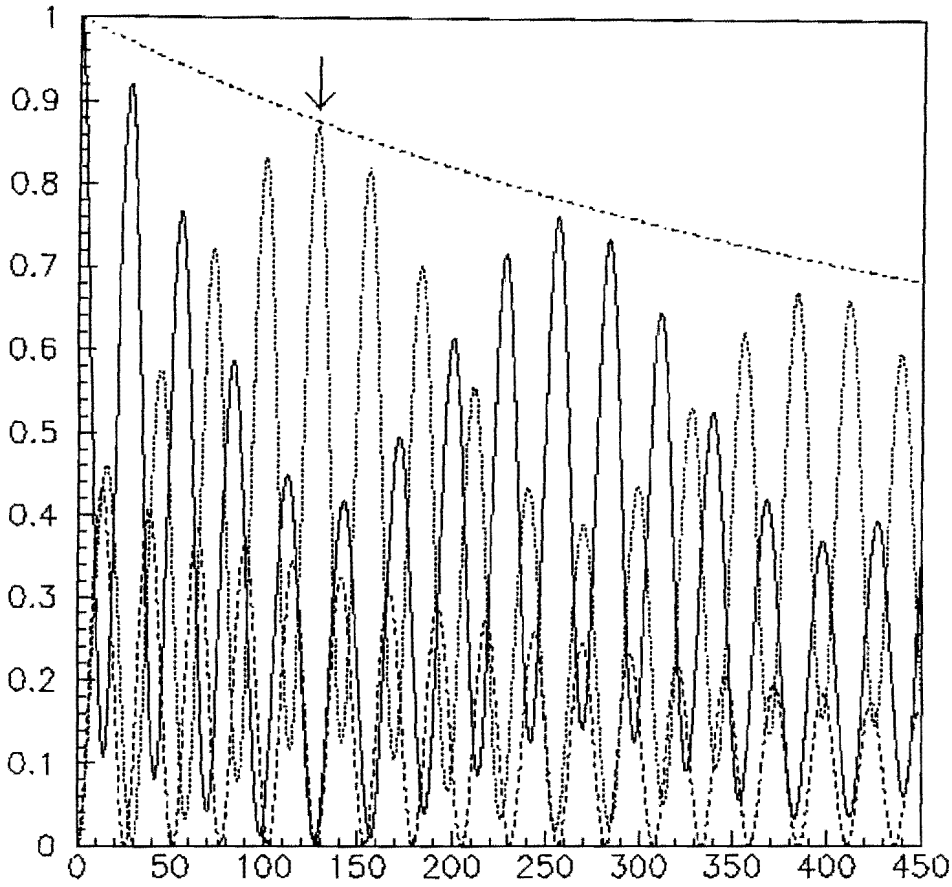

Figure 8: Plot of the probability that an initial long state is found in the long (solid), medium (dashed), or short (dotted) level as a function of the flight distance in cm in zero field. The sum of the three probabilities (dash-dot) shows the decline due to radiative decay. Note that a state that was pure long at $x = 0$ is almost pure short (arrow) at $x = 128\,\mathrm{cm}$, when only 12% of the states have decayed.

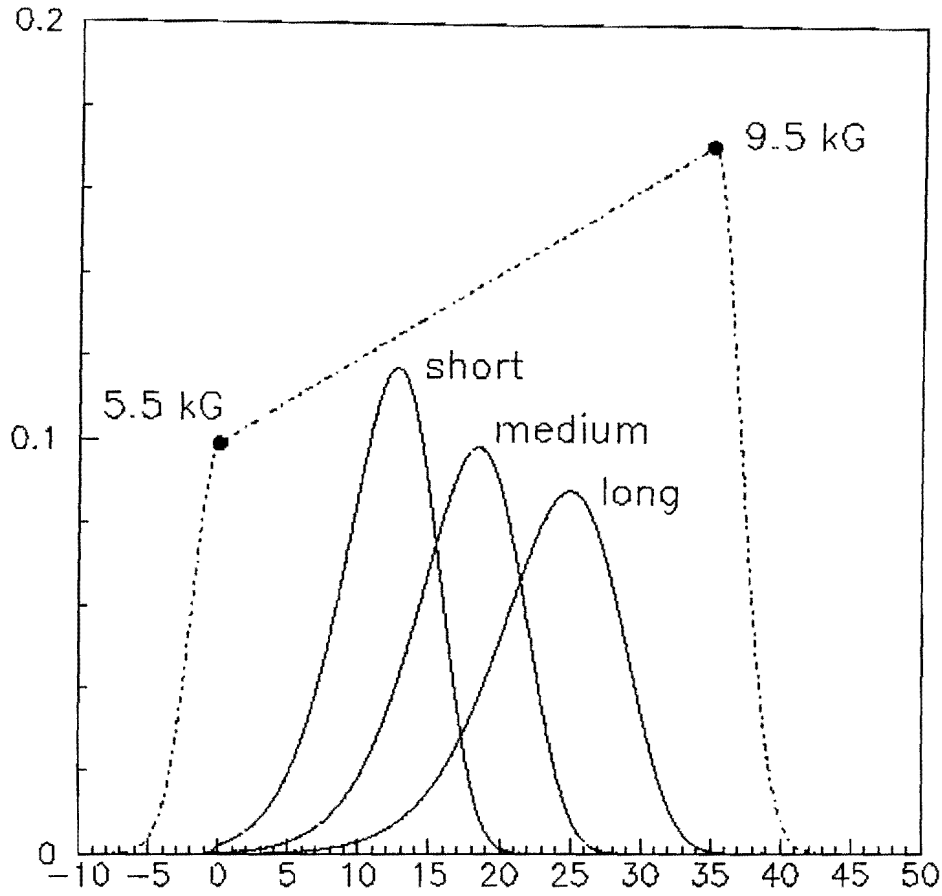

Figure 9: The probability distribution dP/dy [cm^{-1}] for the ionization in the second magnet of a short, medium, or long state, as a function of the depth y in cm. The field profile of the magnet is shown as the dashed line. The total probabilities that a short, medium, or long state ionizes in the magnet are respectively 0.976, 0.942, and 0.963. A long state ionizes with greater probability than does a medium state, though a long state has further to fly before it ionizes, because it has half the rate of radiative decay.

Fermi National Accelerator Laboratory

FERMILAB-Pub-97/426-E
E862

Measuring the Antihydrogen Lamb Shift with a Relativistic Antihydrogen Beam

G. Blanford et al.
The E862 Collaboration

Fermi National Accelerator Laboratory
P.O. Box 500, Batavia, Illinois 60510

December 1997

Submitted to *Physical Review D*

Operated by Universities Research Association Inc. under Contract No. DE-AC02-76CH03000 with the United States Department of Energy

Disclaimer

Distribution

Measuring the Antihydrogen Lamb Shift with a Relativistic Antihydrogen Beam

G. Blanford, K. Gollwitzer, M. Mandelkern, J. Schultz, G. Takei, and G. Zioulas
University of California at Irvine, Irvine, California

D. C. Christian
Fermilab, Batavia, Illinois

C. T. Munger
Stanford Linear Accelerator Center, Stanford University, Stanford, California 94309
(December 18, 1997)

We propose an experiment to measure the Lamb shift and fine structure (the intervals $2s_{1/2} - 2p_{1/2}$ and $2p_{1/2} - 2p_{3/2}$) in antihydrogen. A sample of 5000 antihydrogen atoms at a momentum of 8.85 GeV/c suffices to measure the Lamb shift to 5% and the fine structure to 1%. Atomic collisions excite antihydrogen atoms to states with $n = 2$; field ionization in a Lorentz-transformed laboratory magnetic field then prepares a particular $n = 2$ state, and is used again to analyze that state after it is allowed to oscillate in a region of zero field. This experiment is feasible at Fermilab.

11.30.Er, 25.43.+t, 36.10.-k

I. INTRODUCTION

The CPT theorem predicts the existence of the antimatter counterpart of every physical state. Antimatter states corresponding to elementary particles and some light nuclei have been observed. Until recently no antimatter atomic or molecular state had been detected. A CERN group [1] reported antihydrogen candidates in 1995. We have obtained a background-free sample of antihydrogen atoms in a Fermilab experiment [2]. Study of antimatter-matter symmetry is interesting as the only test of CPT invariance, a principle that is fundamental to our description of elementary particle interactions.

CPT invariance states that the product of the charge conjugation (C), parity (P) and time reversal (T) operations is an exact symmetry of nature. It is the minimal condition for the existence of antiparticles within quantum field theory. It can be derived from very general principles, specifically that a quantum field theory should be constructed from fields that belong to finite-dimensional representations of the Lorentz group, have local interactions invariant under the proper Lorentz group, and be described by a Hermitian Lagrangian. The predictions of the CPT theorem are that particle and antiparticle states have equal masses, spins, and lifetimes, and equal but opposite charges and magnetic moments. The most stringent tests made to date are the equality of the electron and positron g factors [3] to 2.1 parts in 10^{12}, and the equality of $|e/m|$ for the proton and antiproton [4] to 1.5 parts in 10^9. An indirect determination [5] of the $K^0-\bar{K}^0$ fractional mass difference yields a limit of $9{\cdot}10^{-19}$. Matter-antimatter symmetry has thus been studied in leptons and bound states of quarks. Using antimatter atoms, we can perform CPT tests of systems comprised of multiquark states (nuclei) interacting electromagnetically with leptons (electrons).

The hydrogen atom is the best studied of all physical systems and extremely precise measurements of its spectrum have been made, the best of which is of the $1s-2s$ interval [6] to 3.4 parts in 10^{13}. Antihydrogen at rest would be the ideal system for the study of CPT in atomic interactions and experiments are planned at CERN, where a new facility [7] is in construction, to emulate the high precision measurements made in hydrogen.

We have developed a way to measure the spectrum that uses instead antihydrogen in a relativistic atomic beam. Our method of measuring the energy differences between the $n = 2$ levels is an exact analog to the method of measuring the K_L-K_S mass difference by studying the time dependence of K^0 semileptonic decays. We describe an experiment which is feasible at the Fermilab Antiproton Accumulator with an antihydrogen beam at 8.85 GeV/c. The simulation described below is based on the parameters of that machine.

II. OVERVIEW OF EXPERIMENT

In our Fermilab experiment [2] we formed antihydrogen atoms by passing antiprotons stored in the Fermilab Antiproton Accumulator through a hydrogen gas jet target. We identified antihydrogen atoms, with no background, by requiring a coincidence between a positron signal and an antiproton tracked in a high-resolution ($5{\cdot}10^{-4}$) magnetic spectrometer. We now propose to pass the antiprotons through a high-Z gas jet target in order to take advantage of the Z^2 rise [8,9] in the cross section. Antihydrogen atoms will be identified using a coincidence between an antiproton tracked in a similar magnetic spectrometer and a positron tracked in a lower resolution detector.

Antihydrogen atoms emerge from the Accumulator in the $1s$ state. The atoms are next excited by their passage through a thin foil mounted in a magnetic field. The electric field experienced by the atoms in their rest frame ionizes all of the excited states except those in the long-lived Stark level with $n = 2$. A long-lived state can be represented as a coherent sum of the zero-field $n = 2$ states, which are split by the fine structure and Lamb shift. The atoms next pass through a region with zero magnetic field, in which the state accrues phase differences between its zero-field components, resulting in "vacuum regeneration" of the medium-lived and short-lived Stark states. The reappearance of these states changes the point where the atom will ionize in a second magnet, since the short- and medium-lived states ionize in smaller magnetic fields. By measuring where the atoms ionize, as a function of the flight distance in zero field, we can determine the fine structure and Lamb shift splittings. The ionization point may be found by tracking the positron and antiproton.

III. METHOD

In a strong electric field the 8 states with $n = 2$ separate into 3 Stark levels, each of which has a different rate of field ionization. At fields large enough that the rates of field ionization are much larger than the rate ($6.27{\cdot}10^8\,\mathrm{s}^{-1}$) at which the $2p$ state decays radiatively, the lifetimes of the levels are in the ratios of roughly 25:5:1. We will label these levels and the states that belong to them as long, medium, and short, respectively. The difference in the lifetimes allows us to pass a beam of atoms with $n = 2$ through an electric field and cause all but the long level to ionize.

If this beam passes suddenly into a 'drift' region of zero field, a surviving long state projects onto the zero-field eigenstates as

$$\Psi(t{=}0) = \sqrt{\tfrac{1}{2}}\,|s_{1/2}\rangle + \sqrt{\tfrac{1}{6}}\,|p_{1/2}\rangle - \sqrt{\tfrac{1}{3}}\,|p_{3/2}\rangle\ . \qquad (1)$$

The state then evolves forward in time as

$$\begin{aligned}\Psi(t) = {} & \sqrt{\tfrac{1}{2}}e^{-iE(s_{1/2})t/\hbar}|s_{1/2}\rangle \\ & + \sqrt{\tfrac{1}{6}}e^{-iE(p_{1/2})t/\hbar-(\Gamma/2)t/\hbar}|p_{1/2}\rangle \\ & - \sqrt{\tfrac{1}{3}}e^{-iE(p_{3/2})t/\hbar-(\Gamma/2)t/\hbar}|p_{3/2}\rangle\ . \end{aligned} \qquad (2)$$

Here Γ is the width (fwhm) of the $2p$ state due to its radiative decay.

The state that is pure long at $t = 0$ evolves into a superposition of long, medium, and short. If the beam suddenly enters another electric field, this superposition is again projected onto the Stark states. A state with a large projection onto long will typically penetrate deeply into the second electric field before ionizing; a state with a large projection onto short will typically ionize immediately; and a state with a large projection onto medium will usually ionize at an intermediate depth. By measuring the distribution of the depth at which the state ionizes, as a function of the time spent in zero field, we can determine the zero-field splittings of the $n = 2$ states.

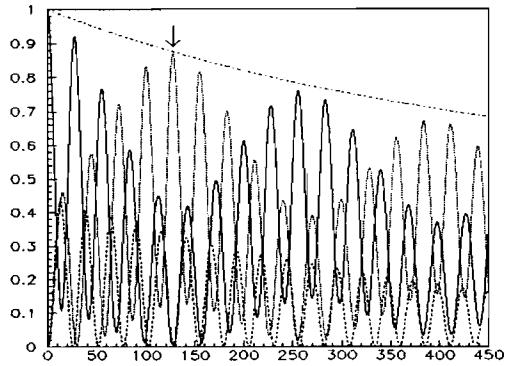

FIG. 1. Plot of the probability that an initial long state is found in the long (solid), medium (dashed), or short (dotted) level as a function of the flight distance in cm in zero field. The sum of the three probabilities (dash-dot) shows the decline due to radiative decay. Note that a state that was pure long at $x = 0$ is almost pure short (arrow) at $x = 128$ cm, when only 12% of the states have decayed.

The probabilities that an initial long state may be found in a long, medium, or short state are

$$\begin{aligned} P\begin{pmatrix}\text{long}\\ \text{short}\end{pmatrix} = {} & \left[\tfrac{1}{2} \pm e^{-x/2}\left(\tfrac{1}{3}\cos fx + \tfrac{1}{6}\cos lx\right)\right]^2 \\ & + \left[e^{-x/2}\left(\tfrac{1}{3}\sin fx - \tfrac{1}{6}\sin lx\right)\right]^2 \end{aligned} \qquad (3)$$

and

$$P(\text{medium}) = \tfrac{2}{9}e^{-x}\big(1 - \cos(f + l)x\big)\ , \qquad (4)$$

where $x = \Gamma t/\hbar$ and

$$\begin{aligned} l &= \big(E_{s_{1/2}} - E_{p_{1/2}}\big)/\Gamma > 0\ ; \quad \text{and} \\ f &= \big(E_{p_{3/2}} - E_{s_{1/2}}\big)/\Gamma > 0\ . \end{aligned} \qquad (5)$$

These oscillating functions are plotted in Fig 1. The fast oscillation, of period 28.5 cm, in the probability of a long state is due to the $2s_{1/2} - 2p_{3/2}$ splitting, and the slow modulation, of period 267 cm, is due to the Lamb shift splitting. Since the long state can oscillate into a virtually pure short state, and since the ionization rates of these states differ by a factor of roughly 25, the oscillation is easy to detect.

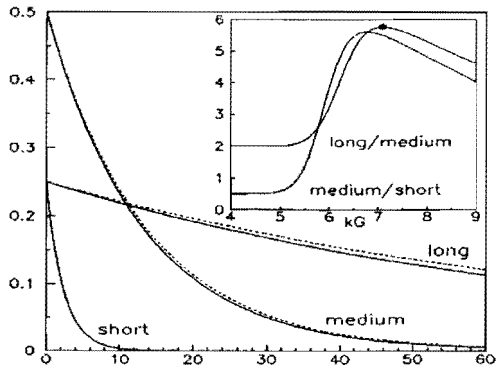

FIG. 2. Plot of the probabilities that an incoherent mixture of $n = 2$ states is found in the short, medium, or long level, as a function of the flight distance in cm in a transverse laboratory magnetic field of 7.090 kG. The solid curves show the result of the full simulation; the dashed curves show the result in the approximation that the three levels decay separately with decay rates set by field ionization alone. The difference can be perceived only for the medium and long states; it is due almost entirely to the omission of the appropriate fraction (1/2, 1, or 1/2) of the $2p$ radiative decay rate appropriate for each of the three levels. At the field of 7.090 kG ratio of the decay length of long to that of medium has its maximum value of 5.8 (insert).

We now analyze a design for an experiment where the large ($\sim 2{\cdot}10^9$ V/cm) electric fields required are provided by the Lorentz transform of laboratory magnetic fields into the rest frame of an 8.85 GeV/c antihydrogen beam, such as has been produced at FNAL [2].

Accurate calculations are required of the rates of field ionization for the different levels with $n = 2$. The eigenvalue problem for the Schrödinger hydrogen atom in an electric field (nearly) separates in parabolic coordinates; the ionization rates have been intensively studied theoretically and are available to 6 decimals at discrete values of the electric field [10]. They are also available as (asymptotic) series in powers of the applied field, times an exponential factor; while not convergent, these series [11] allow accurate interpolation. The code used in our simulations evolves the 8×8 density matrix for the states with $n = 2$ through the perpendicular electric and magnetic fields that result from the Lorentz transform of a transverse laboratory magnetic field. The Wigner-Weisskopf formalism is used to include the losses due to field ionization and to radiative decay; the linear [12] Stark and Zeeman perturbations are included, as are the fine-structure and Lamb shift splittings, but the hyperfine splitting is neglected.

We begin the experiment by making antihydrogen atoms by circulating an antiproton beam stored in the Fermilab Antiproton Accumulator through a high-Z gas jet. The atoms emerge from the Accumulator in the $1s$ state, and roughly 8% of the atoms are excited [13] to states with $n = 2$ by passing them through a very thin ($60\,\mu$gm/cm^2) carbon or equivalent polypropylene foil, while most of the other atoms remain in the $1s$. The $1s$ atoms are ionized in a second, thicker foil far downstream and counted to monitor the relative luminosity.

We assume that collisions in the foil produce the eight $n = 2$ states with equal probability [14]. The subsequent evolution of these states in a uniform, transverse magnetic field of 7.090 kG is shown in Fig. 2. The medium [15] and short states ionize rapidly, leaving a nearly pure long state. The ionization rates are sensitive functions of the applied magnetic field and the beam momentum. Changing either by 0.1% will change the $1/e$ lengths for ionization in this magnet by 1.8%. The unusual sensitivity arises because field ionization is a tunneling process and so its rate varies exponentially with the applied electric field. This sensitivity does not pose a problem because the momentum of the Accumulator is controlled to 0.02%.

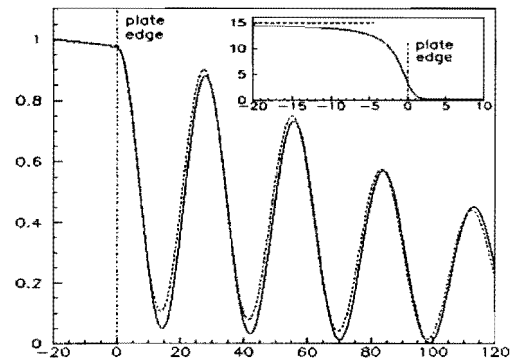

FIG. 3. The probability as a function of coordinate y [cm] that a state that is pure long at $y = -20$ cm remains long as it passes into the drift region. The field profile used (insert) is that of a transverse field of 15 G that is screened by a pair of parallel, infinitely permeable plates that have their edges at $y = 0$ and are separated by 4 cm. (It is convenient to study the field from a pair of plates, instead of from a cylinder, because the profile may be obtained in almost closed form [21] by conformal mapping.) The solid curve is the result of the full simulation; the dashed curve is the approximation that for $y < 0$ the long state does not mix and may only decay radiatively, and at $y = 0$ begins to oscillate in zero field as given by Eq. (3).

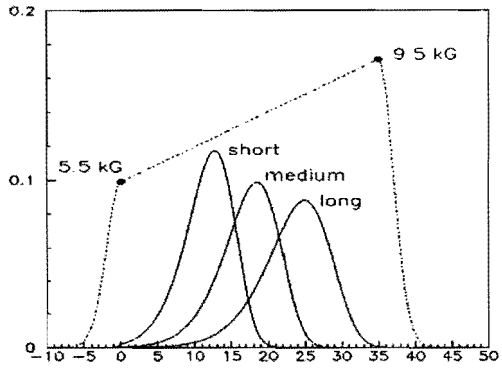

FIG. 4. The probability distribution $dP/dy\,[\mathrm{cm}^{-1}]$ for the ionization in the second magnet of a short, medium, or long state, as a function of the depth y in cm. The field profile of the magnet is shown as the dashed line. The total probabilities that a short, medium, or long state ionizes in the magnet are respectively 0.976, 0.942, and 0.963. A long state ionizes with greater probability than does a medium state, though a long state has further to fly before it ionizes, because it has half the rate of radiative decay.

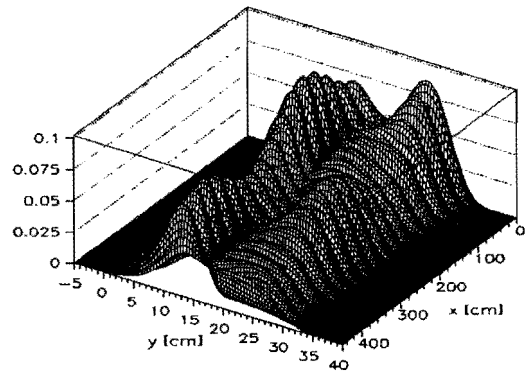

FIG. 5. The differential probability $dP/dy\,[\mathrm{cm}^{-1}]$ for a positron to appear at coordinate y in the second magnet, as a function of the drift distance x in cm. The fast oscillation (period 28.5 cm) is due to the $2s_{1/2}$–$2p_{3/2}$ oscillation, while the slow modulation in its amplitude (period 267 cm) is due to the $2s_{1/2}$–$2p_{1/2}$ oscillation. The overall loss in probability with increasing x is due to radiative decays in the drift region, which produce atoms in the $1s$ state that consequently do not ionize in the second magnet.

In the drift region, laboratory transverse magnetic fields must be $\leq$ 3 mG to avoid Stark mixing. Longitudinal magnetic fields involve only the weaker Zeeman mixing and are not boosted and so can be much larger, $\leq$ 10 G. A sufficiently field-free region of adjustable length can be provided by a set of telescoping μ-metal cylinders.

The transition from the first magnet to the drift region must now be tailored so that the $n = 2$ Stark states undergo a non-adiabatic transition. A key observation is that in a field below 5 kG the $n = 2$ states do not ionize (see Fig. 4); and in a field above 3 G the Stark splitting is so much larger than the fine structure splitting that the long, medium, and short states do not mix. It is only in the range 3 G to 3 mG that a sudden fall of the magnetic field must be engineered; qualitatively we expect that the fields must be made to fall off in a distance short compared to the spatial period of the fine-structure oscillation, or 28.5 cm. Figure 3 shows how the transition can be made non-adiabatic using a simple structure that is large enough to accommodate the antihydrogen beam.

For a second magnet, Fig. 4 shows the separate probability distributions for the point of ionization of the short, medium, and long states. The distribution of ionization points is shown as a function of drift distance in Fig. 5. An antihydrogen atom ionizes into an equal-velocity positron and antiproton, both of which we track to determine the ionization point. Gulley *et al.* [16] used a similar technique to ionize and count states with $n \geq 3$ in an 800 MeV neutral hydrogen beam.

We simulate an experiment by integrating luminosity sufficient for 100 long states, on average, to emerge from the first magnet. The $1/e$ decay length of the $2p$ state sets a natural limit [17] to the useful length of a drift region, and we wish to sample a set of drift distances separated by substantially less than the spatial period of the fine structure oscillation. Accordingly we divide the luminosity evenly between 101 equally spaced drift distances ranging from from 0 to 450 cm. An average of 80 ionizations occur. The complicated function shown in Fig. 5 is fit to the data using the Method of Maximum Likelihood [18]. In keeping with the results of the Fermilab experiment, we assume that there is no background. There are three variables fit: the shifts of the $2s_{1/2}$ and $2p_{1/2}$ states toward the $2p_{3/2}$ state, relative to their values in hydrogen; and the number of long states that emerge from the first magnet.

Shown in Fig. 6 are the results of the fit for 20 simulated experiments. The experiment is sensitive at the 1σ level to independent shifts of either the $2s_{1/2}$ or the $2p_{1/2}$ state equal to 0.5 and 0.9 radiative widths of the $2p$ state. Equivalently, the experiment measures the antihydrogen Lamb shift (the $2s_{1/2}$–$2p_{1/2}$ splitting) to 5% and the fine structure (the $2p_{1/2}$–$2p_{3/2}$ splitting) to 0.9%. Assuming that an interaction that violates CPT will shift the $2s$ state but not the $2p$, the experiment is sensitive to a

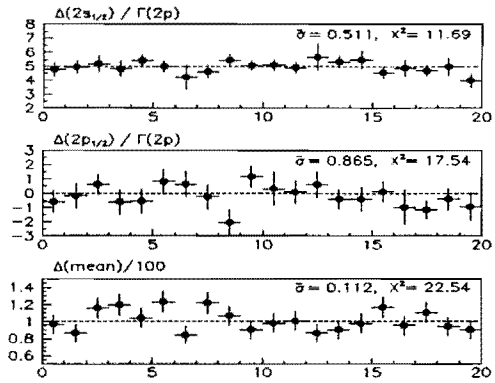

FIG. 6. Results of a three-parameter likelihood fit to 20 simulated experiments that measure the fine structure and Lamb shift of antihydrogen. Shown are the shifts toward the continuum of the $2s_{1/2}$ and $2p_{1/2}$ states, relative to their values in hydrogen, in units of the $2p$ radiative width. Shown too is the ratio of the number of long states let into the drift region to the set value of 100. The vertical error bars are the standard 1-sigma errors estimated for each variable y from the value of $\partial^2 \ln L/\partial y^2$ evaluated at the minimum. Dashed lines show the values set in the simulation; a CPT-violating shift of the $2s_{1/2}$ state of +5 is identified cleanly.

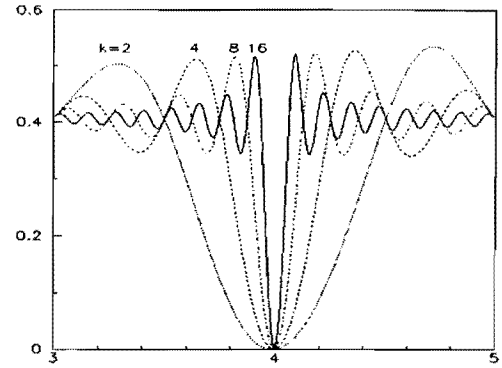

FIG. 7. The (negative) log of the expectation value of the likelihood function for 1 event distributed as $1+\cos(\omega' t)$ over a time T. The plots are shown as a function of the estimate ω for the parameter $\omega' = 4$, for $T = 2\pi k/\omega'$ where k is an integer. The curves are shifted vertically to have the common value 0 at their common global minimum at $\omega = 4$. The width of the central minimum scales as $1/k$.

shift of $5{\cdot}10^{-8}$ of the $2s$ binding energy.

It is at first sight surprising that so small a number of detected events suffices to determine the energy splittings precisely. We model this effect by using the likelihood method to form an estimate ω of a true frequency ω' from N events distributed as $1+\cos(\omega' t)$ over a time interval T. The log of the expectation value of the likelihood function in this simple model can be found analytically, and for $N = 1$ equals

$$\log L = \log\left[1 + \frac{\sin\omega T}{\omega T} + \frac{\sin\omega' T}{\omega' T} + \frac{\sin(\omega+\omega')T}{2(\omega+\omega')T} + \frac{\sin(\omega-\omega')T}{2(\omega-\omega')T}\right] - \log\left[1 + \frac{\sin\omega T}{\omega T}\right] - \log\left[1 + \frac{\sin\omega' T}{\omega' T}\right] . \quad (6)$$

This function is plotted as a function of ω in Fig. 7. It oscillates about a central minimum at the expected value with a separation of the central and adjacent local minima of $3\pi/T$. The rms uncertainty σ_ω is found from the expectation of the second derivative of $-\log L$ and is given by

$$\frac{\sigma_\omega}{\omega} = \left[\frac{3}{N}\frac{1}{((2\pi k)^2 - 9)}\right]^{1/2} . \quad (7)$$

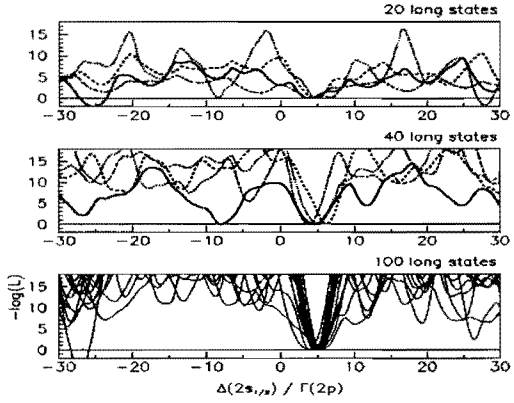

FIG. 8. The (negative) log-likelihood function near the minimum, plotted as a function of the shift of the $2s_{1/2}$ state towards the continuum in units of the $2p$ radiative width. Each figure shows functions for different experiments with the same number of long states entering the drift region; the functions are shifted vertically so that they have the common value zero at the local minimum nearest the preset CPT-violating shift of +5. The third figure shows the functions for the same 20 simulated experiments as in Fig. 6.

Here $k = \omega' T/2\pi$ is the number of periods over which observation extends. For $k = 1$ and $N = 100$, we find that σ_ω/ω is 3%, roughly equal to the error we have simulated for the Lamb shift. The resolution improves as $1/T$ for a fixed number of events because of the increasing lever arm by which each event constrains the phase of the oscillation. For $k = 16$ we find that σ_ω/ω is 0.2%, roughly equal to the error we have simulated for the fine structure. An experiment must have a sufficient number of events N to resolve the central minimum.

For the antihydrogen experiment we similarly obtain adjacent local minima in the (negative) log-likelihood function that may lead to a spurious fit for a sufficiently small number of events. The effect of these minima on the 20 simulated experiments, and on experiments with yet smaller expected numbers of events, is examined in Fig. 8. Experiments with 100 long states expected are almost always free of such extra minima; experiments with 40 are usually free, while experiments with as few as 20 often have such minima, and moreover will often lack the statistical power to exclude the possibility of no shift of the $2s$ state if in fact a shift is present. Demanding 100 long states for a practical experiment therefore seems reasonable, since an experiment may still succeed if only 40 are produced. Given that 8% of an antihydrogen beam in the $1s$ state may be excited by collisions in a foil to states with $n = 2$, and that 1/4 of these are long states, we assert that an experiment can be done on a sample of 5000 atoms of antihydrogen.

IV. EXPERIMENTAL MATTERS

A. Rate

Antihydrogen is formed in antiproton-nucleus collisions by the process $\bar{p}Z \rightarrow Z\bar{H}e^-$. We have measured [2] the cross section at 5.7 GeV/c for $Z = 1$ to be $1.12 \pm 0.14 \pm 0.09$ pb. The cross section for forming antihydrogen in the $1s$ state at 8.85 GeV has been estimated [8,9] to lie between $1.5Z^2$ and $5.0Z^2$ pb; for Xenon the lower estimate gives 4.4 nb. The design of the Accumulator allows antihydrogen formed in states with $n = 2$ to contribute to the flux of $1s$ antihydrogen from the machine, increasing the effective cross section by another $\sim 13\%$ to 4.9 nb. The beam antiprotons also interact by inelastic processes and by large-angle elastic scattering, both resulting in immediate beam loss, and by multiple small-angle elastic scattering. This multiple scattering increases the size and momentum spread of the beam and leads to beam loss when this beam "heating" exceeds the cooling capability of the machine. We take a gas jet density such that, at the FNAL Antiproton Accumulator, there are no beam losses due to heating, giving an instantaneous luminosity of approximately $10^{29}\,\mathrm{cm}^{-2}\mathrm{sec}^{-1}$. We estimate the effective Xe cross section for beam loss at this machine to be 3 b so that 1.6 antiprotons per 10^9 consumed result in antihydrogen. The Accumulator is expected to stack antiprotons at 10^{11} per hour during Fermilab Collider Run 2. At the above luminosity we consume 1% of these antiprotons, giving in parasitic operation ~ 40 antihydrogen atoms per day. Of these 8% are excited to $n = 2$ of which 1/4 are in a long state, giving 0.8 atoms in a long state per day. Accumulating the needed 100 long states takes four months of running. Electron cooling, which delivers far greater cooling power, is planned for the Fermilab Recycler [19]. It may be possible to operate with much greater luminosity in that machine.

The FNAL Antiproton Accumulator is able to circulate protons in the direction opposite to the normal circulation of antiprotons. Relativistic atoms of hydrogen are formed not only by the reaction $pZ \rightarrow ZHe^+$ but by the radiative capture of a target electron, a process which has the relatively large cross section [20] of 344 pb at 8.85 GeV/c. By moving the experiment and reversing the polarity of its magnets, the Lamb shift and fine structure splittings of hydrogen can be measured by the same apparatus as that used for antihydrogen. Such an experiment would be useful in analyzing possible systematic effects.

B. Event detection

The Fermilab experiment [2] demonstrated that observation of an antiproton track within $1 \cdot 10^{-2}$ of the Accumulator momentum, in coincidence with a positron, detects antihydrogen with no background. As in that experiment, the antiproton is detected in a magnetic arm instrumented with 1 mm wire chambers with a momentum resolution of $5{\cdot}10^{-4}$. The 4.8 MeV/c positron is detected in a thin, vertical detector with coordinate sensitivity in the beam direction, positioned in the second magnet about 2 cm from the beam axis. At FNAL, the antihydrogen beam is contained (95%) in a circle of 1 cm radius. The positron, emerging from the ionization point in the beam direction, orbits with a cyclotron radius of about 2 cm in the horizontal plane and so traverses the detector twice, the midpoint of the hits giving the longitudinal coordinate of the ionization with a precision of 1 mm rms. A multiwire proportional chamber with windows and cathodes made of 25 micron aluminized mylar ($\sim 5{\cdot}10^{-5}$ radiation lengths) is a suitable detector. Straw tubes, silicon-strip detectors and scintillating fibers are alternative technologies. The antiproton track furnishes the horizontal distance between the point of ionization and the positron detector to better than 1 mm rms, giving an additional constraint. A poorer measurement of the longitudinal coordinate of the ionization point (1 cm rms) comes from the antiproton track, limited by the 0.2 mr divergence of the antihydrogen beam.

V. CONCLUSIONS

We describe an experiment to measure the Lamb shift and fine structure (the intervals $2s_{1/2} - 2p_{1/2}$ and $2p_{1/2} - 2p_{3/2}$) in antihydrogen. In four months of parasitic operation at the FNAL Antiproton Accumulator, these intervals can be measured to 5% and 1% respectively.

This work was partially supported by the U. S. Department of Energy.

---

[1] G. Baur, G. Boero, S. Branksiepe, A. Buzzo, W. Eyrich, R. Geyer, D. Grzonka, J. Hauffe, K. Kihan, M. LoVetere, M. Macri, M. Mossburger, R. Nellen, W. Oelert, S. Passagio, A. Pozzo, K. Rohrich, K. Sachs, G. Schepers, T. Sefzick, R. S. Simon, R. Stratmann, F. Stinzig, and M. Wolke, Phys. Lett. B**368**, 251 (1996).

[2] G. Blanford, D. C. Christian, K. Gollwitzer, M. Mandelkern, C. T. Munger, J. Schultz, and G. Zioulas, submitted to Phys. Rev. Lett.

[3] R. S. Van Dyck, Jr., P. B. Schwinberg, and H. G. Dehmelt, Phys. Rev. Lett. **59**, 26 (1987).

[4] G. Gabrielse, D. Phillips, W. Quint, H. Kalinowsky, G. Rouleau, and W. Jhe, Phys. Rev. Lett. **74**, 3544 (1995). Note the number in equation 2 should read 0.999 999 998 5(11); see [5], p. 561.

[5] The Particle Data Group, Phys. Rev. D **54**, 1 (1996); see p. 412.

[6] Th. Udem, A. Huber, B. Gross, J. Reichert, M. Prevedelli, M. Weitz, and T. W. Hänch, Phys. Rev. Lett. **79**, 2647 (1997).

[7] Design Report CERN/PS 96-43 (AR). See also http://www.cern.ch/PSdoc/acc/ad/index.html.

[8] C. A. Bertulani and G. Baur, "Antihydrogen production and accuracy of the equivalent photon approximation," HEPPH-9711273, Nov. 1997; e-Print Archive hep-ph/9711273.

[9] C. T. Munger, S. J. Brodsky, and I. Schmidt, Phys. Rev. D**49**, 3288 (1994); C. T. Munger, S. J. Brodsky, and I. Schmidt, Hyperfine Interactions **76**, 175 (1993).

[10] R. J. Damburg and V. V. Kolosov, J. Phys. B **9**, 3149 (1976); see Table 2. R. J. Damburg and V. V. Kolosov, J. Phys. B11, 1921 (1978); again see Table 2.

[11] H. J. Silverstone, E. Harrell, and C. Grot, Phys. Rev. A **24**, 1925 (1981).

[12] In fields of about 7 kG the Stark effect mixes states with $n = 2$ and states with $n \neq 2$ substantially, and so including only the linear Stark and Zeeman effects is not adequate to find accurate eigenvalues. It is adequate for finding accurate decay rates, however, because the Stark splitting so dominates the fine structure, Lamb, and Zeeman splittings that the Stark states decouple. The error in the eigenvalues then appears only in irrelevant phase factors.

[13] B. Gervais, C. O. Reinhold, and J. Burgdörfer, Phys. Rev. A**53**, 3189 (1996). The $n = 2$ yield ($\sim 8 - 10\%$) and optimum target thickness for a beam kinetic energy of 800 MeV/c is estimated from Fig. 10. In the Born approximation all cross sections scale as $1/\beta^2$, so at 8.85 GeV/c the yield is the same and the target thickness merely greater by a factor of 1.4.

[14] We further assume that this remains so if the foil is in a 7 kG magnetic field, when the Stark effect mixes substantially states with $n = 2$ with states with $n \neq 2$. The cross sections for the various excitation, rearrangement, and ionization collisions may however be expected to change from their zero-field values. We may avoid making this further assumption by leaving the foil in zero field and putting the first magnet a short distance downstream.

[15] Half of the remaining medium states are the $2p_{3/2}$, $m_j = \pm 3/2$ states that do not oscillate in zero field and are unlikely to confuse the oscillating pattern of ionization that results from the long states.

[16] M. S. Gulley, P. B. Keating, H. C. Bryant, E. P. MacKerrow, W. A. Miller, D. C. Rislove, S. Cohen, J. B. Donahue, D. H. Fitzgerald, S. C. Frankle, D. J. Funk, R. L. Hudson, R. J. Macek, M. A. Plum, N. G. Stanciu, O. B. van Dyck, C. A. Wilkinson, and C. W. Planner, Phys. Rev. A**53**, 3201 (1996).

[17] As shown in Eqns. (3-4), the probability of an oscillation between long and short falls as $e^{-x/2}$, not e^{-x}. An experiment therefore may be able to use a drift region of order not once but twice the $1/e$ decay length of the $2p$ state, or 900 cm.

[18] R. Barlow, Nucl. Instrum. and Meth. in Phys. Res. A **297**, 496 (1990); J. Orear, University of California Report UCRL-8417 (1958). In keeping with standard numerical practice, we minimize the negative log-likelihood rather than maximize the log-likelihood.

[19] G. Jackson, FERMILAB-TM-1991, Nov., 1996.

[20] V. B. Berestetskii, E. M. Lifshitz, and L. P. Pitaevskii, Vol. 4 of "Quantum Electrodynamics, Course of Theoretical Physics," 2nd ed., (Pergamon, New York, 1982), pp. 207-216.

[21] N. Levinson and R. M. Redheffer, "Complex Variables," (Holden-Day, Inc., 1970), pp. 295-297.